



HAL
open science

A study of low temperature mechanical properties and creep behaviour of polypropylene using a new sub-ambient temperature nanoindentation test platform

Jian Chen, Gerard A Bell, Hanshan Dong, James F Smith, Ben D Beake

► **To cite this version:**

Jian Chen, Gerard A Bell, Hanshan Dong, James F Smith, Ben D Beake. A study of low temperature mechanical properties and creep behaviour of polypropylene using a new sub-ambient temperature nanoindentation test platform. *Journal of Physics D: Applied Physics*, 2010, 43 (42), pp.425404. 10.1088/0022-3727/43/42/425404 . hal-00569726

HAL Id: hal-00569726

<https://hal.science/hal-00569726>

Submitted on 25 Feb 2011

HAL is a multi-disciplinary open access archive for the deposit and dissemination of scientific research documents, whether they are published or not. The documents may come from teaching and research institutions in France or abroad, or from public or private research centers.

L'archive ouverte pluridisciplinaire **HAL**, est destinée au dépôt et à la diffusion de documents scientifiques de niveau recherche, publiés ou non, émanant des établissements d'enseignement et de recherche français ou étrangers, des laboratoires publics ou privés.

A study of low temperature mechanical properties and creep behavior of polypropylene using a new sub-ambient temperature nanoindentation test platform

Jian Chen¹, Gerard A. Bell¹, Hanshan Dong¹, James F. Smith², Ben D. Beake²

1. School of Metallurgy and Materials, University of Birmingham, Birmingham, B15 2TT, UK,

2. Micro Materials Ltd, Willow House, Yale Business Village, Ellice Way, Wrexham, LL13 7YL, UK

Abstract

Mechanical properties and creep behaviour of an atactic-polypropylene (aPP) have been studied in the vicinity of its glass transition temperature (-18°C) via a nanoindentation platform integrated with a sub-ambient temperature capability. All low temperature tests were validated by measurements on a fused silica reference sample from 25°C to -30°C. The fused silica results showed virtually invariant elastic modulus with temperature over this range consistent with literature measurements by sonic resonance. Hardness and elastic modulus of aPP increased as the test temperature decreased and the amorphous regions went through the glass transition. The creep behaviour was analysed using two approaches: (i) a logarithmic method, and (ii) the Boltzmann integral method. The results showed that the creep extent decreased as the temperature was reduced, and for the time constants obtained there were upper-limit values at -10°C, about 8°C above the quoted glass transition temperature. The strain rate sensitivity obtained by the logarithmic method also showed a maximum at -10°C.

Keywords

nanoindentation, sub-ambient temperature, polypropylene, creep

1. Introduction

Nanoindentation enables local probing of spatial variations in mechanical properties, time-dependent behaviour, and strain rate dependence. Such knowledge of materials on a small scale is often key to their optimization for practical applications [1-5]. Normally, these tests are carried out under ambient conditions that may not be close to the actual working conditions for many applications. For example, temperature can play an important role in materials properties; indeed, many mechanical properties are strongly temperature-dependent, for instance a system can operate safely at one temperature and fail when the temperature is changed [6-9]. To address this problem,

several approaches have been used to probe the surface properties of materials under their actual service conditions. For example, nanoindentation has been utilized to test polymers, metals and hard coatings at elevated temperatures [9-13], and the results have been correlated with the performance of coatings in extreme applications such as high speed machining.

Similarly, various engineering activities are carried out at sub-ambient temperatures, including aerospace, marine and cryo-machining applications [7, 14-17]. Materials in-service may be subjected to mechanical loading at low temperatures, for instance. For optimization of wear resistance, in particular, it is highly desirable to determine the mechanical properties under true in-service conditions. Although there are macro-scale sub-ambient temperature commercial mechanical testers [7], up until now there have been no reports of low temperature nanoindentation capability.

A popular engineering polymer, polypropylene, is in the rubbery state at room temperature. Its mechanical properties are expected to vary strongly with reducing temperature as it transforms to the glassy state [14, 18-20], i.e. when the material passes through its glass transition temperature. Moreover, polypropylene shows temperature-dependent viscoelastic behaviour under loading. Thus its time-dependence around the glass-rubber transition temperature is also of interest in this study.

In light of the above comments, a newly-developed sub-ambient temperature capability based on the commercial NanoTest platformTM (Micro Materials Ltd. Wrexham, UK) was therefore utilized to investigate the mechanical properties and creep behaviour of polypropylene around its glass-rubber transition temperature. There are several approaches to analyzing nanoindentation creep data. For example, Bower et al. [21] employed a similitude analysis for the stress and strain field during indentation. Applying a transformation method, the stress exponent of the creep response can be obtained from the displacement-time data during the hold period. Likewise, other researchers [22-25] have analysed creep data assuming that the steady-state creep strain rate follows a power law. Of particular significance in this study, two different approaches were adopted to analyse the temperature-dependent creep behaviour of the polypropylene.

2. Experimental

The sub-ambient temperature measurement capability was developed and integrated with the NanoTest instrument in a manner which preserved normal sample motion and operation routines. This nanoindentation instrument employs horizontal loading as described in detail previously [26]. For sub-ambient measurements three key design changes were made: 1) environmental control, 2) cooling on the sample side, 3) cooling on the indenter side. This capability provided cooling of both the sample and

the diamond indenter down to -30°C without water vapour condensation and thermal drift problems. A reference sample (fused silica) was tested to validate this equipment. A schematic of the new system is shown in Figure 1(a). The design used the same methodology – separate thermal control of both indenter and sample to minimise/eliminate heat flow on contact - used in high-temperature nanoindentation [11, 13], which has been successful in performing tests to 750°C . The sample and diamond indenter were attached to thermoelectric coolers (Peltier elements) as shown in Figure 1(b). To eliminate condensation at sub-ambient temperatures, the whole pendulum system was enclosed in a sealed chamber, which was purged with argon gas. This reduced the water vapour concentration to 300ppm (V). The detailed system design is documented elsewhere [27].

The test materials were fused silica and atactic-polypropylene (aPP). The fused silica was obtained from Starna Scientific Ltd. Essex UK. Fused silica is commonly used as a nanoindentation reference material, with a Young’s modulus of 72 GPa. The aPP was obtained from ENSINGER Ltd, Mid Glamorgan, UK [28] with a quoted glass transition temperature of approximately -18°C . A Berkovich indenter was used for all tests. Indentations were load-controlled to different peak loads at various loading rates as shown in Table 1. The loading history included a hold at peak load before unloading in order to minimize the influence of viscoelastic deformation during subsequent unloading. For aPP, this hold period was set to 20s, and displacement data at constant load was collected during this period to analyse the creep response of the aPP. The Oliver and Pharr method [1] was used to extract hardness and elastic modulus values from the unloading data. Unloading rates were set equal to the loading rates. The separation distance between indentations was $35\mu\text{m}$ and each test was repeated 5 times.

Table 1 Nanoindentation test conditions

No.	Sample	Peak Load (mN)	Loading rate (mN/s)	Loading time (s)	Hold period (s)	Temperatures ($^{\circ}\text{C}$)
1	FS	100	5	20	5	RT (25), 0, -10, -20, -30
2	aPP	50	25	2	20	
3	aPP	50	10	5	20	
4	aPP	50	2.5	20	20	
5	aPP	50	1	50	20	

To study the time-dependent behaviour of aPP at different temperatures, the creep data were analysed and fitted using two approaches: (i) the logarithmic method discussed in Refs. 23 and 24, and (ii) the Boltzmann integral method discussed in Refs. 25-27 The logarithmic equation can be expressed as

$$\Delta d = A \ln \left(\frac{t_h}{\tau_L} + 1 \right) \quad (1)$$

where Δd and t_h are the increase in depth and hold time during hold period, A and τ_L are termed the extent parameter and the time constant, respectively. Equation (1) can also be expressed as the creep strain

$$\frac{\Delta d}{d(t_h=0)} = \frac{A}{d(t_h=0)} \ln \left(\frac{t_h}{\tau_L} + 1 \right) \quad (2)$$

where $d(t_h=0)$ is the initial penetration depth at the beginning of the hold (creep) period, $\Delta d/d(t_h=0)$ is the creep strain, $A/d(t_h=0)$ (the dimensionless fractional increase in depth during creep) is known as the strain rate sensitivity parameter [29].

Although only two variables – measures of extent and rate - are used to describe the visco-deformation behaviour, in practice the creep curves normally show a quasi-logarithmic form [30], thus producing an excellent fit to the raw data.. This method can be used not only for linear viscoelastic materials, but also non-linear viscoelastic materials, and with the quality of the fit it is possible to predict the creep response over a relatively long time. In the past, this method has been used for a range of polymer systems to identify changes in creep behaviour with density of cross-linking [26].

The major limitations of this method are that the equation is empirical and does not explicitly take into account differences in the time taken to reach the peak load, though the fitting parameters reflect this. It is not possible to deconvolute the particular contributions of elasticity, plasticity, viscoelasticity and visco-plasticity by this approach.

In other work [31-35], assuming the materials is linear viscoelastic, different combinations of springs and dashpots have been used to simulate the instantaneous elasticity, instantaneous plasticity, viscoelasticity and visco-plasticity. The creep compliance function is then deduced. The penetration depth can be calculated using the Boltzmann integral operator. This methodology has been successfully adapted by Oyen [4, 34-36] to simulate the whole loading and holding curve. However, a better fit required more variables, which can degrade the accuracy of the solution [36]. Compared to the logarithmic method, this needs more time and a careful selection of the initial value to make the iteration converge. In the present study, a free spring in series with a Kelvin parallel spring and dashpot element was used as the temperature effect can be studied using the time constant from the only dashpot. The background of this method is briefly described as follows.

For a conical-pyramidal indenter, the indentation depth can be expressed as

$$h^2(t) = m \cdot \int_0^t J(t-u) \frac{dP}{du} du \quad (3)$$

where $h(t)$ is the penetration depth, m is constant, P is the load, t is the time, u is a dummy variable of integration for time and $J(t)$ is the material's creep function. The creep function $J(t)$ can be expressed as

$$J(t) = c_0 - c_1 \exp\left(\frac{-t}{\tau_B}\right) \quad (4)$$

where c_0 and c_1 are the creep function coefficients, τ_B is the creep time. The solved equation (3) using the creep function of equation (4) gives

$$h(t) = \left(c_0' k t_R - c_1' k \tau_1 \exp\left(\frac{-t}{\tau_B}\right) \left[\exp\left(\frac{t_R}{\tau_B}\right) - 1 \right] \right)^{\frac{1}{2}} \quad (5)$$

where t_R is the loading time, $c_0' = m c_0$ and $c_1' = m c_1$.

3. Results

Fused silica was used as a reference sample and tested from room temperature (25°C) down to -30°C. To ensure isothermal contact conditions, prior to indentation the diamond was held at the specimen surface for 5 to 30s under minimal load. The recorded loading-unloading curves showed good repeatability. The elastic modulus (E) was found to be (72 ± 2) GPa over the temperature range +25 to -30°C which agrees with the data in Ref [37].

The hardness (H) and elastic modulus (E) results of aPP were measured at different loading rates and temperatures. Indentation tests with the highest loading rate 25mN/s (corresponding to only 2s loading time) resulted in approximately 10% higher modulus for all temperatures studied. There was no clear difference in H and E between the three slowest loading rates, 10mN/s, 2.5mN/s and 1mN/s (loading time 5s, 20s and 50s, respectively). The average values of H and E of aPP were therefore determined from these and are shown in Figure 2. It is clear that the hardness and elastic modulus increased as the testing temperature decreased. The scattering of data can be attributed to the relatively high surface roughness of aPP ($R_a \sim 0.67 \mu\text{m}$). To

minimize the effect of the roughness, a high testing load of 50mN was used. The corresponding maximum depth was about 4000 nm, significantly higher than the Ra value.

Figure 3 illustrates a typical quasi-logarithmic creep curve. The curves obtained at all test temperatures were of this conventional, continuous form, with no discrete relaxation events such as those reported by Ngan on PE [38].

Figure 4.a shows typical creep curves at different temperatures after constant loading at a rate of 25mN/s. It can be seen that the initial depth produced before the hold period was reduced upon decreasing the temperature. The creep depth measured at different conditions (temperature and loading rate) is shown in Figure 4.b. It can be seen that the total creep depth during the hold period decreased with decreasing temperature and loading rate.

4. Discussion

4.1 Hardness and elastic modulus on aPP

The elastic modulus values for the fused silica reference sample were essentially independent of the test temperature over the range studied. This result is in agreement with studies using sonic resonance reported by NIST [30], which also show virtually invariant properties of the fused silica over this range. These results provided validation of the performance of the nanoindentation test capability to -30°C.

Figure 2 shows that the hardness and elastic modulus of aPP exhibited the expected strong dependence on the testing temperature. The increase in H and E can be attributed to the transition of the amorphous regions in the semi-crystalline aPP from a 'rubbery' state at room temperature to a 'glassy' state as the temperature was decreased to its glass transition temperature (-18°C). The aPP has appreciable crystallinity, and for that reason the change in the slope of elastic modulus going through the glass transition is less pronounced than it would have been for an amorphous polypropylene. In previous work by one of the authors on PET around glass transition temperature [11] it was found that the changes in elastic modulus against temperature in elevated temperature nanoindentation depended on the sample crystallinity; for the highest crystallinity PET sample at the change was smooth, whilst for lower crystallinity samples the slope changes dramatically. We attribute the lack of strong slope dependence going through glass transition temperature to the high crystallinity of this aPP sample.

The scatter in the measured H and E values of aPP (Figure 2) can be attributed to the high level of surface roughness. This effect was alleviated by employing relatively high loads (and hence penetration depths). At 50mN the maximum depth at peak load

decreased from ~4800nm at 25°C to ~3000nm at -30°C. Tweedie et al. have recently reported that contact loading may increase the glass transition temperature, so that polymers below their bulk glass transition temperature may exhibit significantly higher than expected stiffness, particularly when the penetration depth is under 200nm [37], consistent with other reports of increasing elastic modulus on polymeric materials as the indentation depth is reduced. Brostow et al. [39, 40] also found densification inside the scratching groove for polypropylene, resulting in increased hardness. Tweedie et al. suggest that the contact loading creates an interfacial region of confined molecular mobility, adjacent to the probe, either via intermolecular interactions or via stretching or alignment of macromolecular chains. Nevertheless, the contribution of this modified region to the overall mechanical response of the bulk polymer decreases with increasing contact depth. To exclude this possibility, a series of comparative indentations at the testing load 25mN was also carried out; the resultant values of E were essentially identical to those at 50mN within the experimental error. The measured increase in E at sub-ambient temperatures does not appear therefore to be overestimated due to the decreasing indentation depths at 50mN.

For a time-dependent material, it is important to compensate the creep effects on the measured H and E – such effects can be strong and have been found to give very misleading results in certain circumstances [2, 29]. It has been suggested elsewhere that the combination of a slow loading rate, long hold period and fast unload can minimize artefacts in modulus determination on viscoelastic materials. The hold period (20s) was sufficiently long to avoid the presence of any ‘nose’ shape – as observed by Ngan and others for shorter holding periods [2, 24, 25, 41] – even with the slowest unloading rate of 1mN/s.

In contrast, at the highest load rate of 25mN/s, the peak load was reached in only 2 s and the resultant modulus values were about 10% higher than at the other loading rates for all temperatures. The influence of visco-deformation on the measurement of the unloading contact stiffness has been discussed in [2, 29] and the applicability of the Feng & Ngan compliance correction equation (equation (6)) [2] has been investigated.

$$\frac{1}{S} = \frac{1}{S_u} + \frac{\dot{D}_h}{\left| \dot{P} \right|} \quad (6)$$

where S is the contact compliance, S_u is the elastic contact stiffness at the onset of unloading, \dot{D}_h is the indenter displacement recorded at the end of the hold period, and $\left| \dot{P} \right|$ is the unloading rate at the onset of unloading.

However, after application of this equation the calculated modulus (E_c) showed a much stronger dependence on the loading/unloading rate with a minimum in E_c at 10mN/s - about 40% less than at 1mN/s. It may be attributed to the different loading history up to the unload which resulted in the different microstructure of the time-dependent material at the onset of unload, and so the tip-sample contact stiffness S should be different [25]. The constant hardness and modulus observed on aPP for indentations at 1, 2.5 and 10mN/s suggests that the presence of the 20s hold period was effective in minimizing the influence of viscoelasticity on the measured hardness and modulus for these slower loading rates.

The higher E at 25 mN/s is a result of the smaller depth at the end of loading period (D_{max}). At room temperature, the maximum depth for the loading rate of 25mN/s (~4200 nm) was much less than for the other loading rates of 1 to 10mN/s (4480-4750 nm). The depth after creep for the 25 mN/s tests was extrapolated to 70s using the logarithmic equation to investigate whether the apparently higher E was simply a result of a shorter total loading time before unloading. The corresponding maximum penetration depth was about 4350 nm - considerably less than those from the tests using the slower loading rates. It is possible therefore that the indentation behaviour of polypropylene shows a more complex dependence on loading rate. It could be explained by an increase in yield strength of polypropylene with the strain rate [18]. Thus extra energy could be required for plastic deformation during indentation. Similar behaviour has been observed in uniaxial PET [42].

4.2 Creep analysis

As described in the Experimental section, the creep behaviour was studied using the logarithmic method and Boltzmann integral method. All hold periods were fitted well using the logarithmic equation as shown in Figure 3.

The variation in the creep extent parameter (A) with temperature from indentations with a loading time of 20s is shown in Figure 5. The dimensionless parameter ($A/d(t_h=0)$) has been considered as a measure of strain rate sensitivity [36], which enables meaningful comparisons of different testing conditions. Our results are shown in Figure 6.a. It can be seen that the value of $A/d(t_h=0)$ is between 0.028 and 0.032 over the entire temperature range, with the highest $A/d(t_h=0)$ at -10°C . The creep time constant (τ_L) from the loading time 20s has been plotted against the testing temperatures in Figure 6.b. It is clear that there is also a maximum τ_L value at -10°C .

It has been shown previously that the actual time to reach the maximum load influences the creep kinetics dramatically [30]. When a constant loading rate was considered for each particular temperature, it was found that τ_L increased with increased loading rate, exhibiting a power law relationship as shown in Figure 7.

Clearly, the correlation coefficient (and Figure 3) indicates that the experimental creep data is extremely well described by the logarithmic equation. The fitted creep extent

parameter, A , decreased with decreasing the test temperature. The dimensionless creep strain sensitivity, $A/d(t_h=0)$, and the creep time constant, τ_L , showed upper-limit values appearing at -10°C . At the same time, the creep time constant, τ_L , showed a power law relationship with the loading time.

The creep data has also been fitted using the Boltzmann integral method. The adjusted square of the correlation coefficient (R^2) is shown in Figure 8. We can see that the quality of fit is improved upon decreasing the loading rate.

As shown in Figure 9.a, the time constant (τ_B) also reached a maximum at -10°C . This indicated that both methods are effective for revealing the effect of glass transition on creep. The time constant also strongly depended on the loading rates. Figure 9.b shows that the time constant (τ_B) at -10°C exhibited a power-law relationship with the loading rates, which agrees with the founding using the logarithmic method (Figure 7).

The fitted variables c_0' and c_1' are shown in Figures 10.a and 10.b. We can see that c_0' decreases with the temperature. As c_0' is proportional to the instantaneous elasticity, this is consistent with the measured E (Figure 2) increasing as the temperature decreases. The creep extent (c_1') showed strong dependence on temperature and loading rate, consistent with the fitted creep extent (A) in Figure 5 obtained using the logarithmic equation. More creep occurred for higher loading rates and temperature.

The creep mechanism in polymers is explained by the Eyring theory as proposed by Berthoud et al. and Tweedie et al. [43, 44]. For a creep event to occur, the polymer chains must overcome a potential barrier by thermal activation at a particular reaction rate. At higher temperatures, the thermal barrier is easier to be overcome and thus the movement of the polymer chains, such as translation and rotation becomes easier than at lower temperatures. Therefore, the creep extent parameter (c_1) would be expected to decrease with a decrease in testing temperature. As the variable (c_1') is proportional to c_1 , it decreases with decreasing temperature as shown in Figure 10.b.

We assume that the creep extent (c_1) obeys an Arrhenius relationship:

$$creep_extent = k \exp\left(\frac{-Q}{RT}\right) \quad (7)$$

where k is constant, R is the gas constant, T is the Kelvin temperature and Q is the activation energy. After taking logarithms, the activation energy Q_B (Boltzmann integral method) can be obtained from the slope ($-Q/R$) of the $\ln(c')$ vs. $1/T$ curve as shown in Figure 11. The calculated Q_B is $11.0 \pm 2.9 \text{ kJ/mol}$.

As shown in Figures 6 and 9.a, in the temperature range considered there were maximum values of $A/d(t_h=0)$ and τ_L using the logarithmic method, and τ_B for the

Boltzmann integral method, at -10°C . In reference [43], the creep strain sensitivity ($A/d(t_h=0)$) for a range of amorphous and semi-crystalline polymers was related to the difference between their glass transition (T_g) and testing temperatures. Similarly for the present work, these parameters indicate a property change around T_g .

Although we have only performed nanoindentation measurements at 10°C intervals and cannot resolve the exact temperature at which peak values of $A/d(t_h=0)$, τ_L and τ_B occur, it is notable that the temperature at which we have determined peak values of these parameters, -10°C , is 8°C above the supplier quoted T_g (-18°C) of the studied aPP. As described in reference [19], reported glass transition temperatures for polypropylene are influenced by a wide range of factors, such as sample tacticity, sample crystallinity and chain length, as well as the measurement technique used. In Dynamic Mechanical Analysis measurements (DMA), the peak in tan delta is typically offset to a few degrees higher than the T_g determined from the inflexion point in the storage modulus versus temperature graph [6, 30]. It has been suggested previously that, based on previous ambient and elevated temperature measurements on semi-crystalline and amorphous polymers, changes in $A/d(t_h=0)$ are correlated with changes in the tan delta peak [12]. It is notable that the offset in $A/d(t_h=0)$ (and the time constants) from the glass transition appears the same (typically $\sim 8\text{-}10^{\circ}\text{C}$) for elevated temperature, ambient temperature and sub-ambient nanoindentation measurements for a wide range of polymers.

The peak value of creep parameters at glass transition temperature indicated different creep mechanisms which have been proposed in references [12, 45] correlating the creep rate behaviour with the difference between T_g and the testing temperature ($y = T_g - T$). When the testing temperature is higher than T_g , the free volume mechanism of creep was implicated as there is more free volume available for molecular motions [6, 45, 46]. At lower temperatures (e.g. for $y > 50^{\circ}\text{C}$) brittleness and crack propagation are likely to be the dominant mechanisms of creep [43]. It was suggested that around the T_g , these two creep mechanisms could be weak resulting in the increase in the creep time. Whatever the mechanism, it is clear that the indentation creep kinetics – both extent and rate – subtly vary in the vicinity of the glass transition. The measured hardness from unloading curve analysis is slightly lower than expected at -10°C (Figure 2) and this appears to be consistent with the comparatively enhanced creep at this temperature.

The peak values of $A/d(t_h=0)$ and τ_L for the logarithmic method at -10°C are about 9% and 16% higher, respectively, than the average of the others. The greater increase in τ_L is consistent with the data in [9] that the parameter τ_L was more sensitive than $A/d(t_h=0)$ to changes in the glass transition region. As mentioned above, the average value of τ_L from all the tested temperatures can be fitted well to a power law relationship vs. loading time. This agrees with the finding [12] that the power law fit for aPP is a better fit than a linear relationship and it is not possible to determine a measurable creep cut-off time from the indentation measurements.

5. Conclusions

The hardness and elastic modulus of atactic-polypropylene increased as the testing temperature decreased through the glass transition range and the polymer changed from rubbery to glassy. A temperature reduction of -55°C from room temperature led to a change of about 100% and 150% increments for hardness and elastic modulus, respectively.

The indentation creep behaviour of atactic-polypropylene can be fitted well using both the logarithmic method and the Boltzmann integral method.

- The creep extent (A and c_1') decreased with decreasing test temperature.
- The time constants (τ_L and τ_B) increased with the loading time with a power-law relationship.
- $A/d(t_h=0)$, τ_L and τ_B indicated a creep rate change at -10°C , which is around the glass transition temperature.
- The fit for the Boltzmann integral method was better at lower loading rates.

Acknowledgement:

The authors would like to thank the late Professor Tom Bell for his contribution to the first part of the project. The authors also wish to express their appreciations to Prof. Witold Brostow at University of North Texas for helpful discussions. Finally, the financial support from EPSRC, UK (EP/C535061/1) is gratefully acknowledged.

Figures

Figure 1 (a) NanoTest pendulum assembly and specimen stage with environmental enclosure; (b) Peltier cooling stages on sample and indenter

Figure 2 Averaged hardness and elastic modulus of aPP tested at different temperatures

Figure 3 Superimposed experimental creep data and logarithmic expression. Testing conditions: (i) load 50mN, (ii) loading rate 25mN/s, (iii) temperature -10°C ; Fitting parameters: $A=97.47\text{nm}$, $B=5.46\text{s}^{-1}$; $d(t_h=0)=3088.1\text{nm}$

Figure 4 (a) Illustrative penetration depth during hold period for the loading rate=25mN/s; (b) Increase of penetration depth during hold period at different testing temperatures

Figure 5 Creep extent parameter (A) vs. test temperature fitted using logarithmic equation

Figure 6 (a) Creep strain rate sensitivity ($A/d(t_h=0)$) vs. test temperature and (b) Creep time constant (τ_L) vs. test temperatures fitted using logarithm equation

Figure 7 Superimposed experimental creep time data (τ_L) and the power law fitted dash curve ($y = 0.105x^{0.976}$, $R^2 = 1$)

Figure 8 The results of adjusted R-Square for the Boltzmann integral fitting

Figure 9 (a) Creep time constant (τ_B) vs. test temperatures and (b) Superimposed experimental creep time data (τ_B) vs. loading time fitted using Boltzmann integral equation and the power law fitted dash curve ($y = 4.105x^{0.271}$, $R^2 = 0.962$)

Figure 10 (a) The effect of the testing temperature on the fitted variable c_0' and (b) c_1' using the Boltzmann integral equation

Figure 11 The creep extent (c_1') in the logarithm axis vs. the reciprocal Kelvin temperature

Reference

1. Oliver W.C. and Pharr G.M. 1992 *Journal of Materials Research*, **7**(6): 1564-1583.
2. Feng G. and Ngan A.H.W. 2002 *Journal of Materials Research*, **17**(3): 660-8.
3. Fischer-Cripps A.C. 2006 *Surface and Coatings Technology*, **200**(14-15): 4153-4165.
4. Oyen M.L. and Cook R.F. 2009 *Journal of the Mechanical Behavior of Biomedical Materials*, **2**(4): 396-407.
5. Beake B.D., *Nanomechanical Testing under Nonambient Conditions*. Encyclopedia of Nanoscience and Nanotechnology, ed. H.S. Nalwa. Vol. X. 2010: American Scientific Publishers. 1-6.
6. Beake B.D., Bell G.A., Brostow W., and Chonkaew W. 2007 *Polymer International*, **56**(6): 773-778.
7. Fink M., Fabing T., Scheerer M., Semerad E., and Dunn B. 2008 *Cryogenics*, **48**(11-12): 497-510.
8. Fox-Rabinovich G.S., Beake B.D., Endrino J.L., Veldhuis S.C., Parkinson R., Shuster L.S., and Migranov M.S. 2006 *Surface & Coatings Technology*, **200**(20-21): 5738-42.
9. Bell G.A., Bielinski D.M., and Beake B.D. 2008 *Journal of Applied Polymer Science*, **107**(1): 577-582.
10. Duan Z.C. and Hodge A.M. 2009 *JOM*, **61**(12): 32-36.
11. Gray A. and Beake B.D. 2007 *Journal of Nanoscience and Nanotechnology*, **7**(7): 2530-2533.
12. Gray A., Orecchia D., and Beake B.D. 2009 *Journal of Nanoscience and Nanotechnology*, **9**: 4514-4519.
13. Xia J., Li C.X., and Dong H. 2003 *Materials Science & Engineering A (Structural Materials: Properties, Microstructure and Processing)*, **A354**(1-2): 112-120.
14. Zhu Y., Okui N., Tanaka T., Umemoto S., and Sakai T. 1991 *Polymer*, **32**(14): 2588-2593.
15. Yoshino Y., Iwabuchi A., Onodera R., Chiba A., Katagiri K., and Shimizu T. 2001 *Cryogenics*, **41**(7): 505-511.
16. Yuhno T.P., Vvedensky Y.V., and Sentyurikhina L.N. 2001 *Tribology International*, **34**(4): 293-298.
17. Caron I., De Monicault J.M., and Gras R. 2001 *Tribology International*, **34**(4): 217-223.

18. Zrida M., Laurent H., Grolleau V., Rio G., Khlif M., Guines D., Masmoudi N., and Bradai C. Polymer Testing, **In Press, Accepted Manuscript**.
19. Cowie J.M.G. 1973 European Polymer Journal, **9**(10): 1041-1049.
20. Wortmann F.J. and Schulz K.V. 1996 Polymer, **37**(5): 819-824.
21. Bower A.F., Fleck N.A., Needleman A., and Ogbonna N. 1993 Proceedings of the Royal Society of London, Series A (Mathematical and Physical Sciences), **441**(1911): 97-124.
22. XU X., JERONIMIDIS G., ATKINS A.G., and TRUSTY P.A. 2004 Journal of Texture Studies, **35**(1): 11-32.
23. Dutta A.K., Penumadu D., and Files B. 2004 Journal of Materials Research, **19**(1): 158-64.
24. Ngan A.H.W., Wang H.T., Tang B., and Sze K.Y. 2005 International Journal of Solids and Structures, **42**(5-6): 1831-46.
25. Ngan A.H.W. and Tang B. 2009 Journal of Materials Research, **24**(3): 853-62.
26. Beake B.D., Zheng S., and Alexander M.R. 2002 Journal of Materials Science, **37**(18): 3821-6.
27. Bell G.A., Chen J., Dong H., Smith J.F., and Beake B.D. in preparation.
28. ENSINGER, TECAFINE PP Data Sheet, ENSINGER Ltd, Wilfried Way, Tonyrefail, Mid Glamorgan, CF39 8JQ.
29. Chudoba T. and Richter E. 2001 Surface & Coatings Technology, **148**(2-3): 191-198.
30. Beake B. 2006 Journal of Physics D: Applied Physics, **39**(20): 4478-4485.
31. Fischer-Cripps A.C. 2004 Materials Science and Engineering A, **385**(1-2): 74-82.
32. Odegard G.M., Gates T.S., and Herring H.M. 2005 Experimental Mechanics, **45**(2): 130-136.
33. Mencik J., He L.H., and Swain M.V. 2009 Journal of the Mechanical Behavior of Biomedical Materials, **2**(4): 318-325.
34. Oyen M.L. 2006 Philosophical Magazine, **86**(33-35): 5625-41.
35. Oyen M.L. 2005 Journal of Materials Research, **20**(8): 2094-100.
36. Oyen M.L. 2007 Acta Materialia, **55**(11): 3633-9.
37. Munro R.G., Elastic Moduli Data for Polycrystalline Ceramics, in NISTIR, National Institute of Standards and Technology. 2002, National Institute of Standards and Technology.
38. Li J. and Ngan A.H.W. 2010 Scripta Materialia, **62**(7): 488-491.
39. Brostow W., Chonkaew W., Rapoport L., Soifer Y., Verdyan A., and Soifer Y. 2007 Journal of Materials Research, **22**(9): 2483-2487.
40. Brostow W., Chonkaew W., Mirshams R., and Srivastava A. 2008 Polymer Engineering & Science, **48**(10): 2060-2065.
41. Ngan A.H.W. and Tang B. 2002 Journal of Materials Research, **17**(10): 2604-10.
42. Beake B.D., Goodes S.R., Smith J.F., and Gao F. 2004 Journal of Materials Research, **19**(1): 237-47.
43. Berthoud P., G'Sell C., and Hiver J.M. 1999 Journal of Physics D (Applied Physics), **32**(22): 2923-2932.
44. Tweedie C.A. and Van Vliet K.J. 2006 Journal of Materials Research, **21**(6): 1576-1589.
45. Brostow W., Deshpande S., Pietkiewicz D., and Wisner S.R. 2009 e-Polymers, **no. 109**.
46. Brostow W. and Hagg Lobland H.E. 2010 Journal of Materials Science, **45**(1): 242-250.

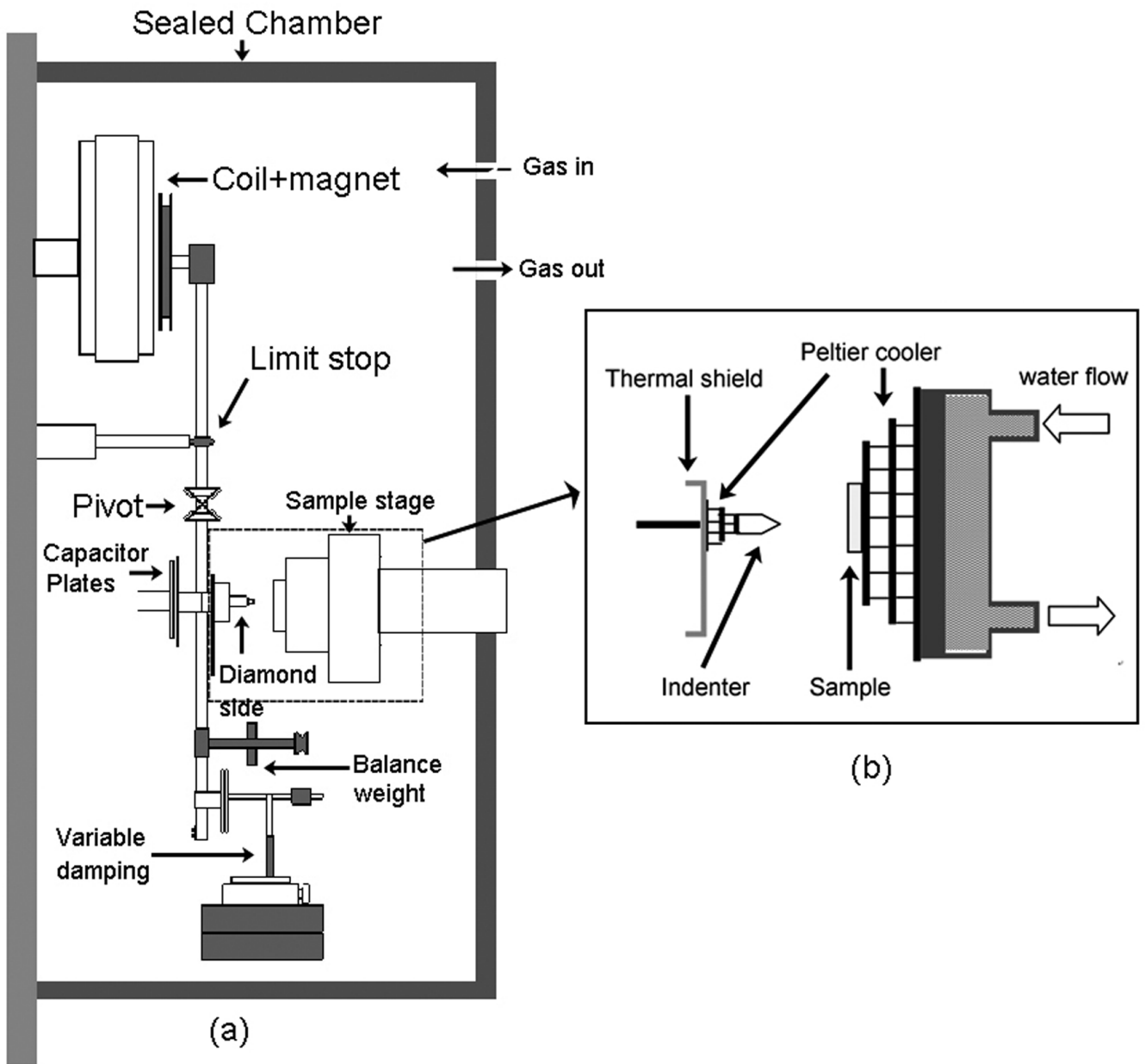


Figure 1 (Figure1(a)_ (b).tif)

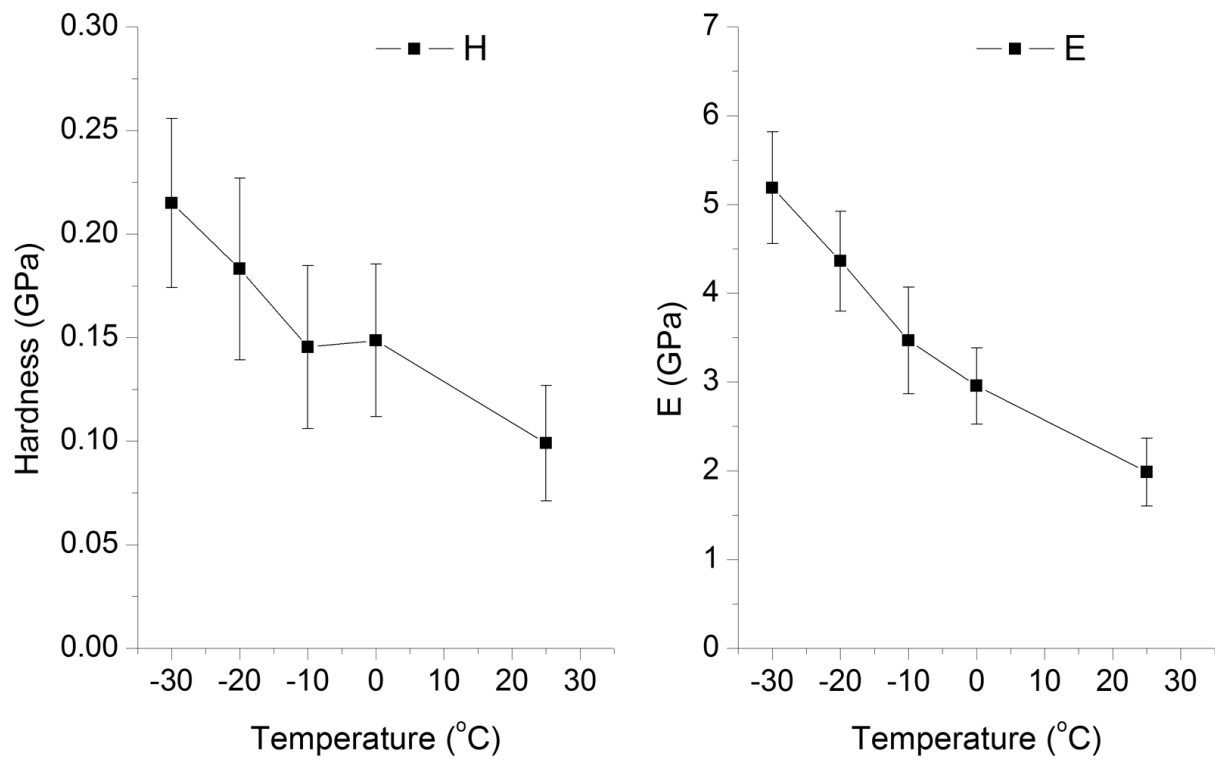


Figure 2 (Figure2.tif)

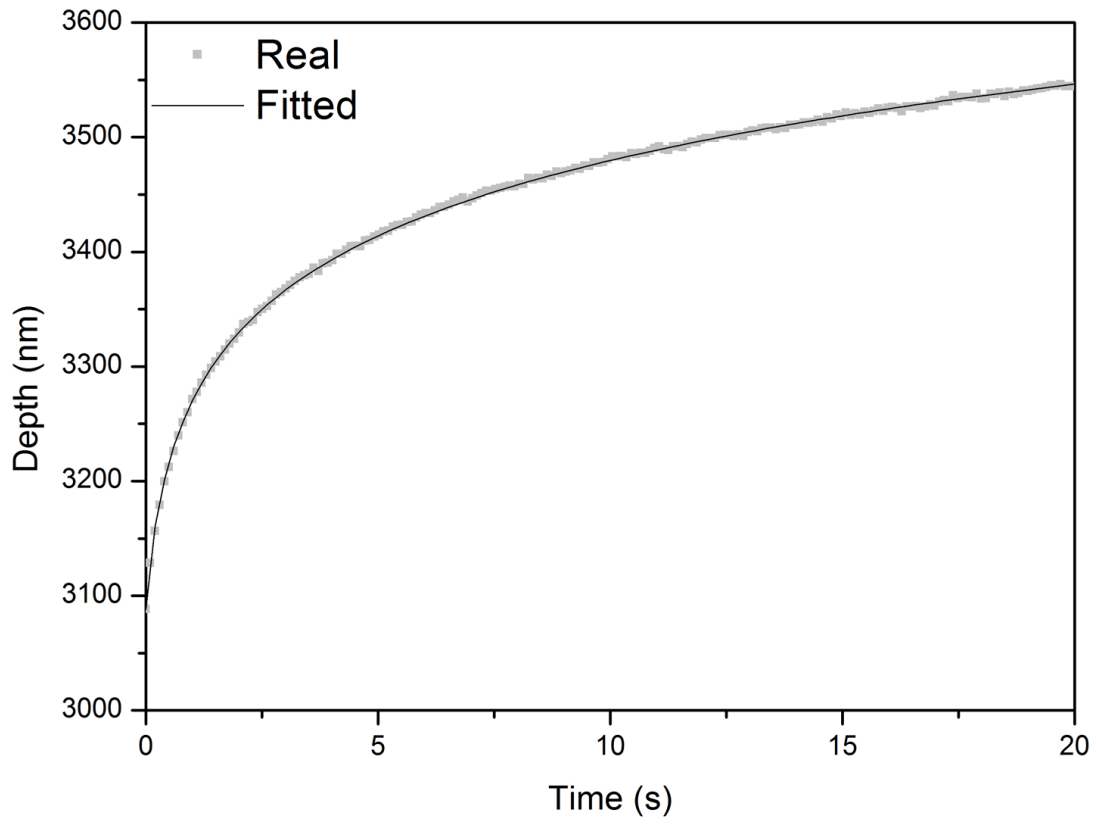


Figure 3 (Figure3.tif)

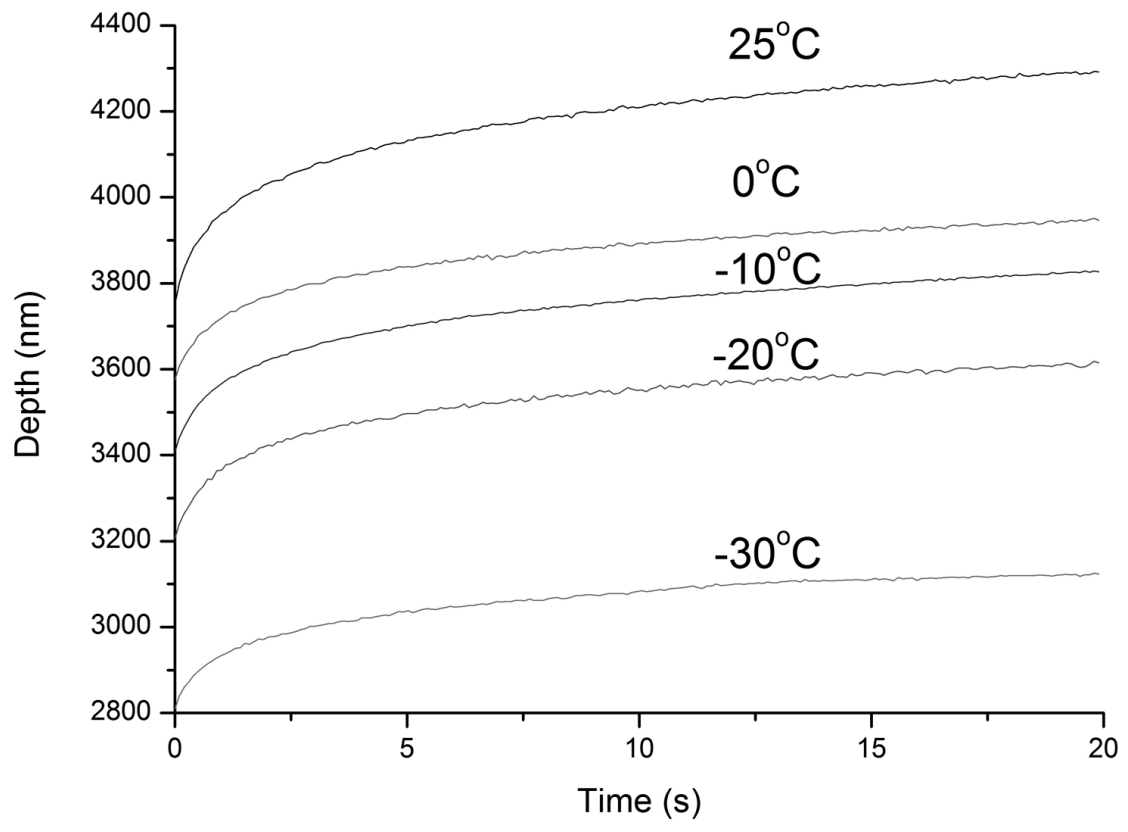


Figure 4a (Figure4(a).tif)

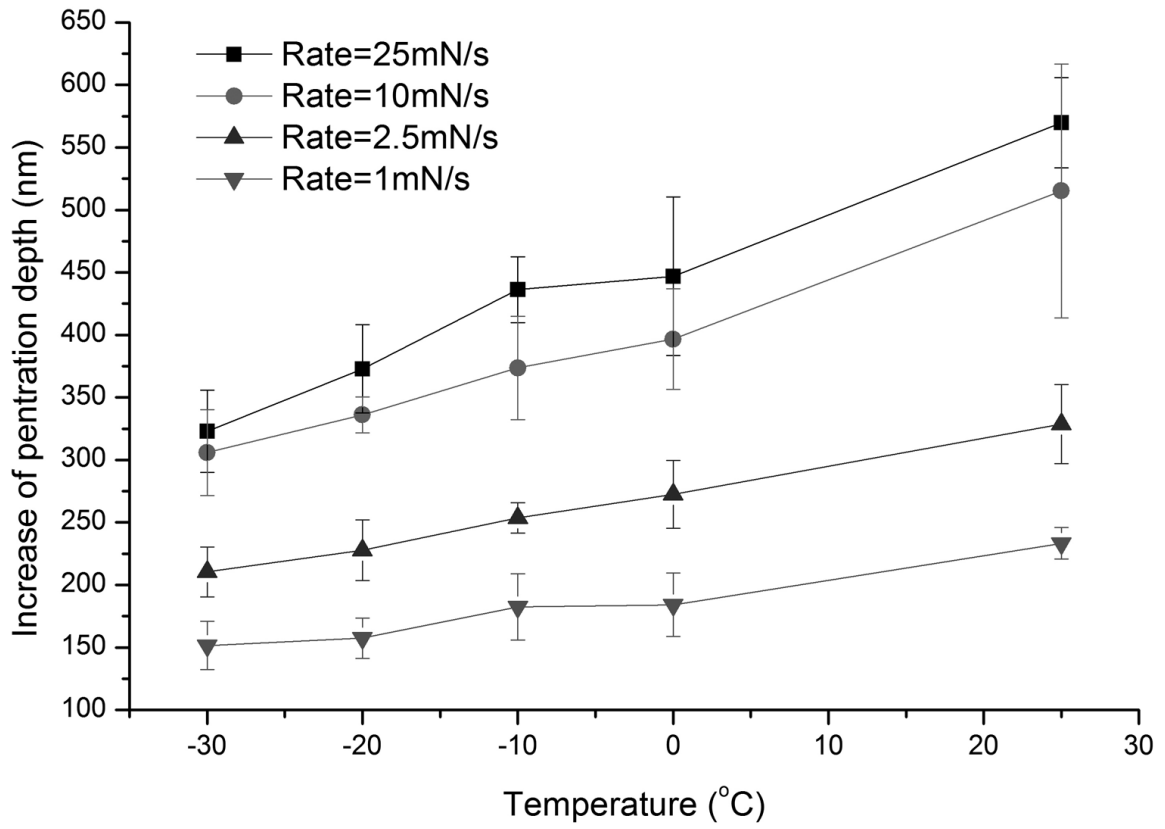


Figure 4b (Figure4(b).tif)

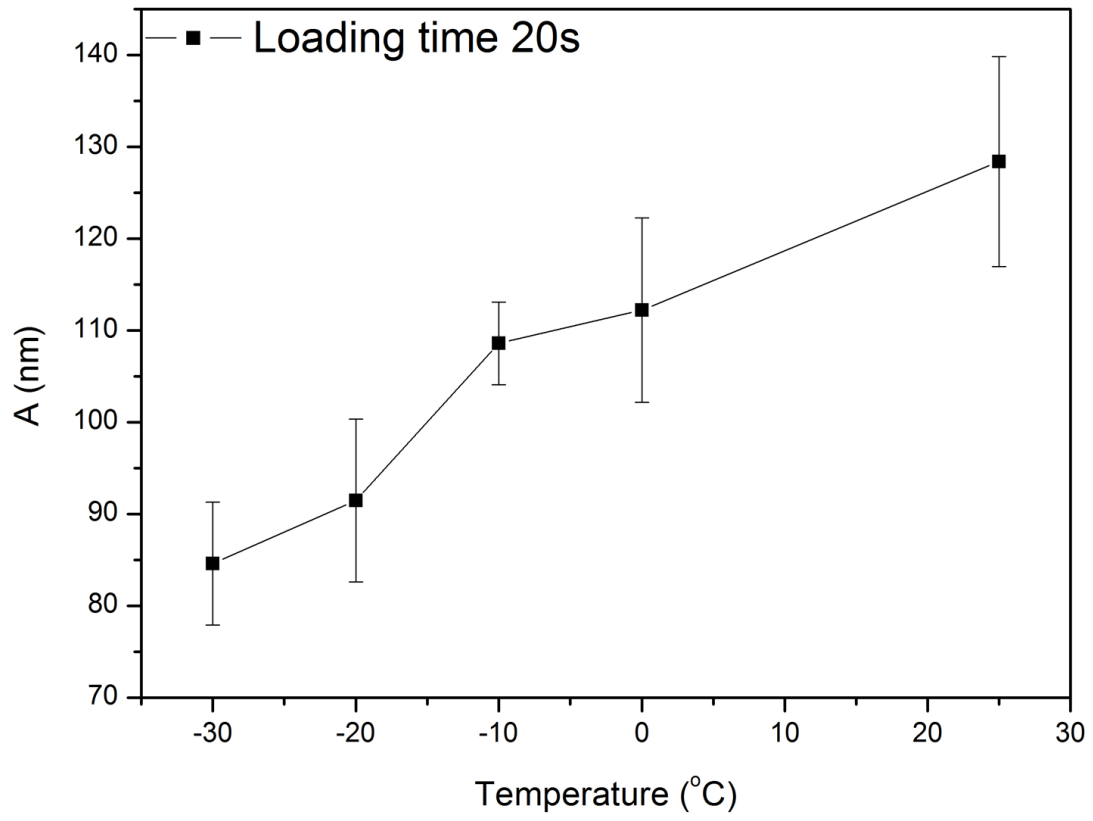


Figure 5 (Figure5.tif)

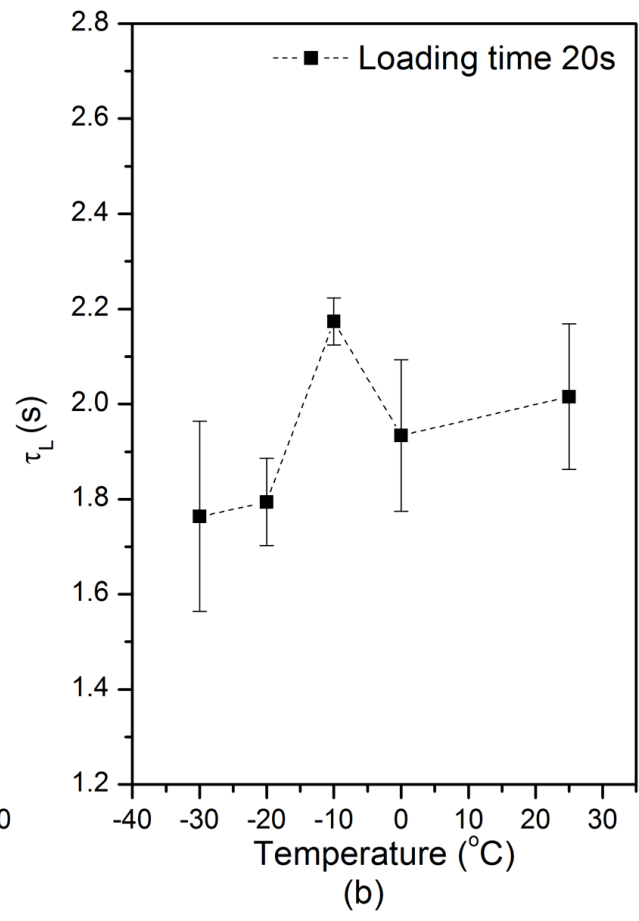
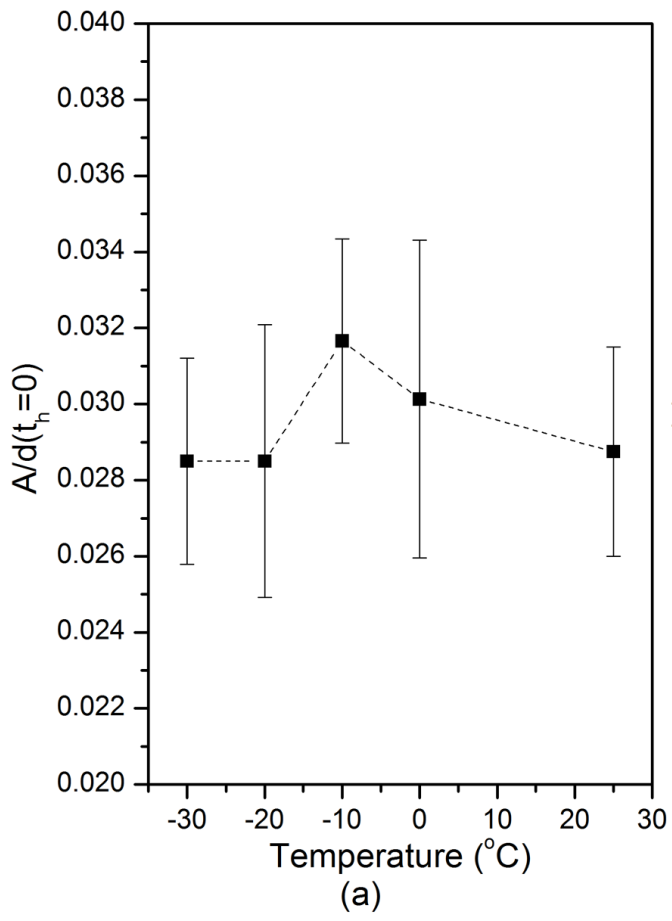


Figure 6 (Figure6(a)_ (b).tif)

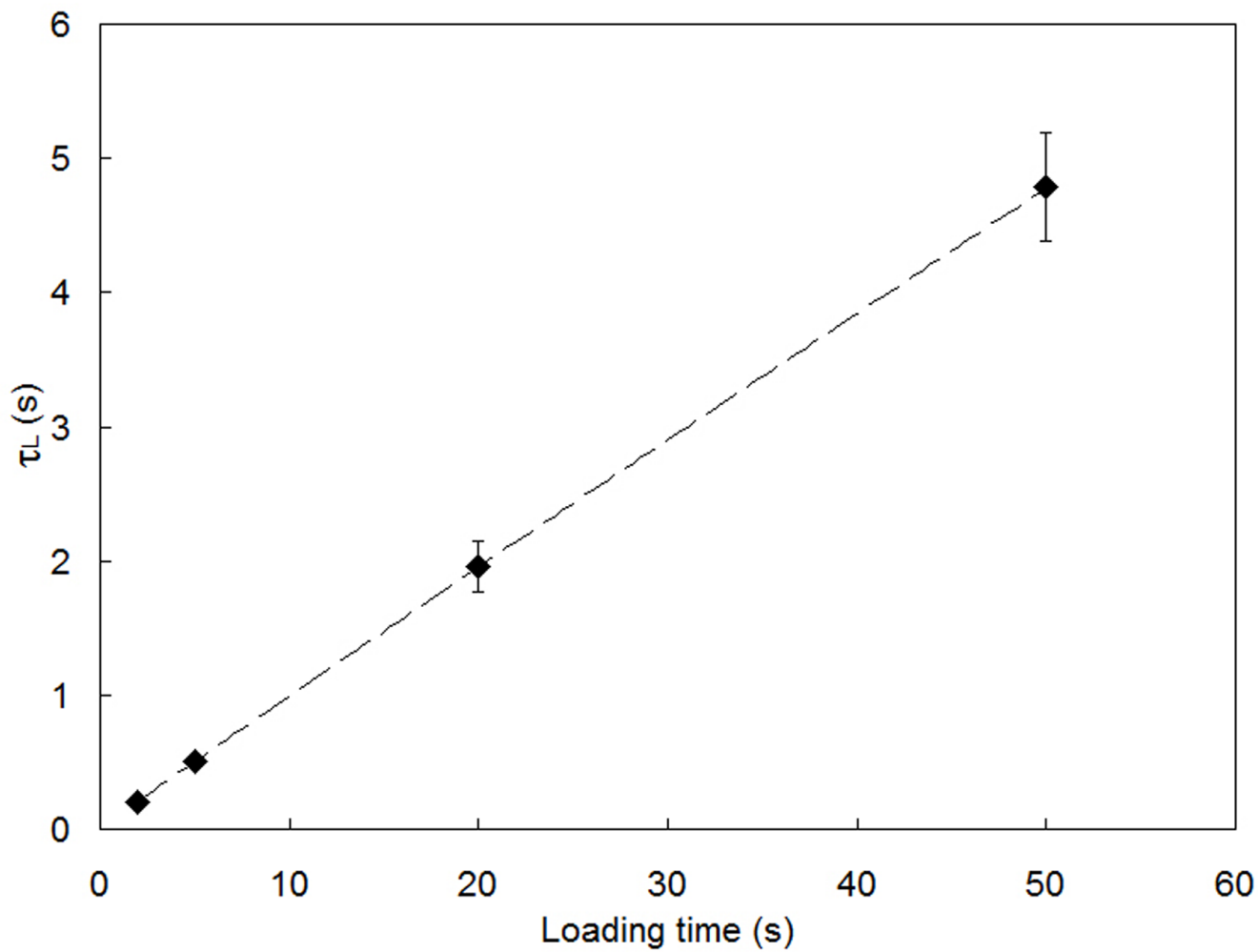


Figure 7 (Figure7.tif)

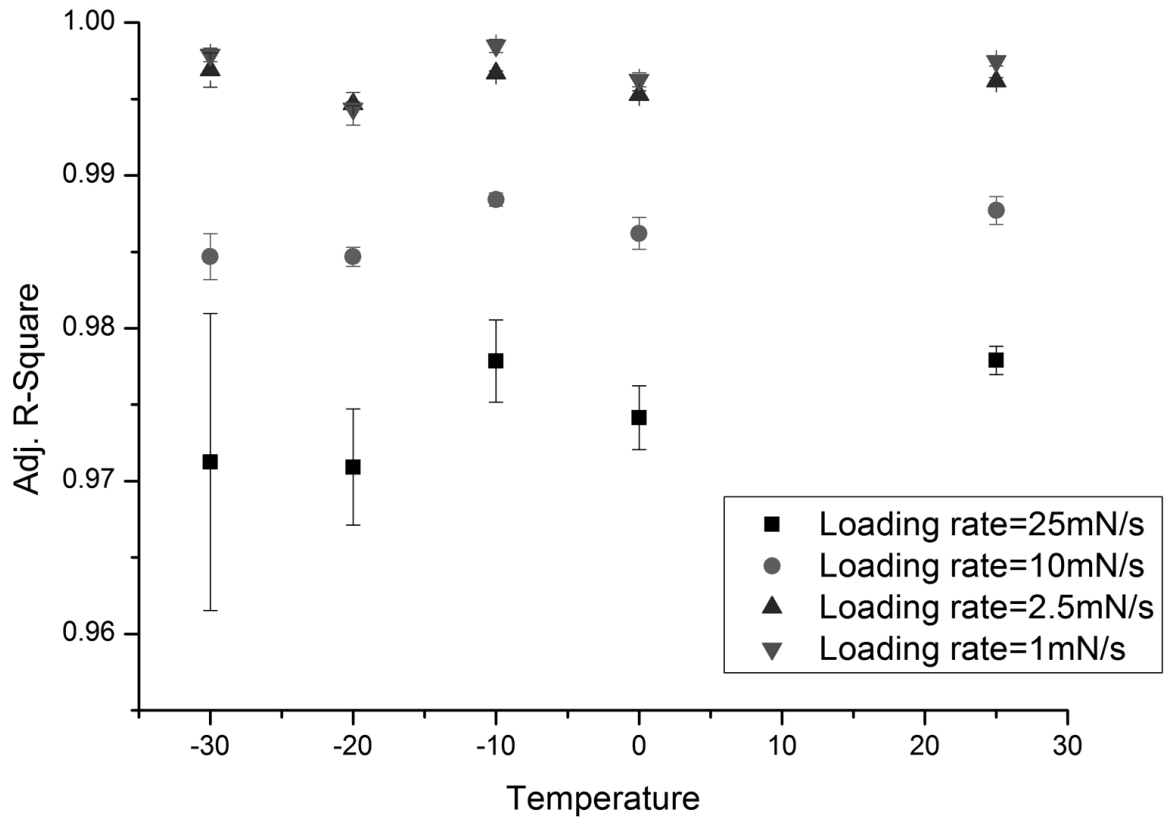


Figure 8 (Figure8.tif)

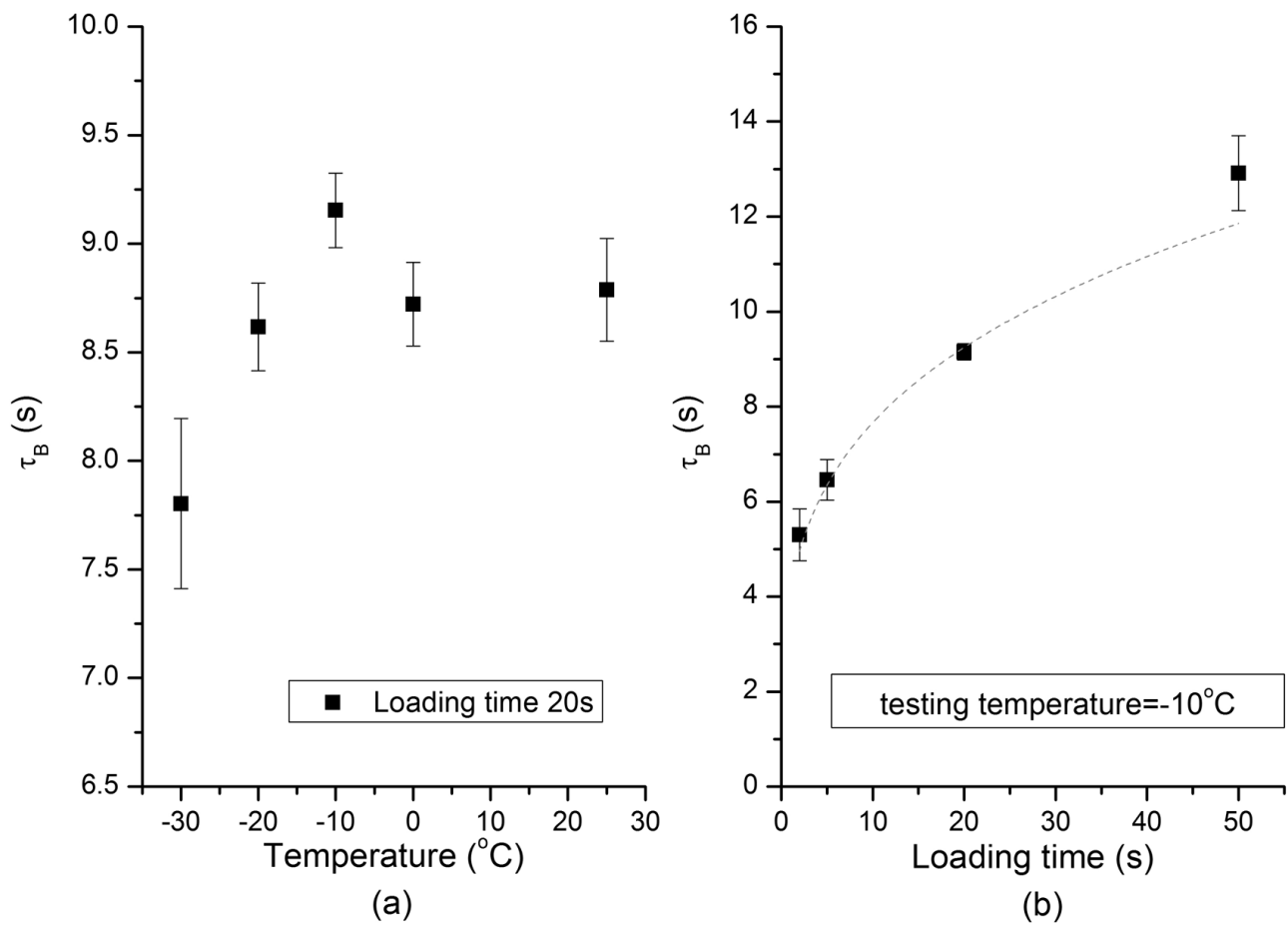


Figure 9 (Figure9(a)_ (b).tif)

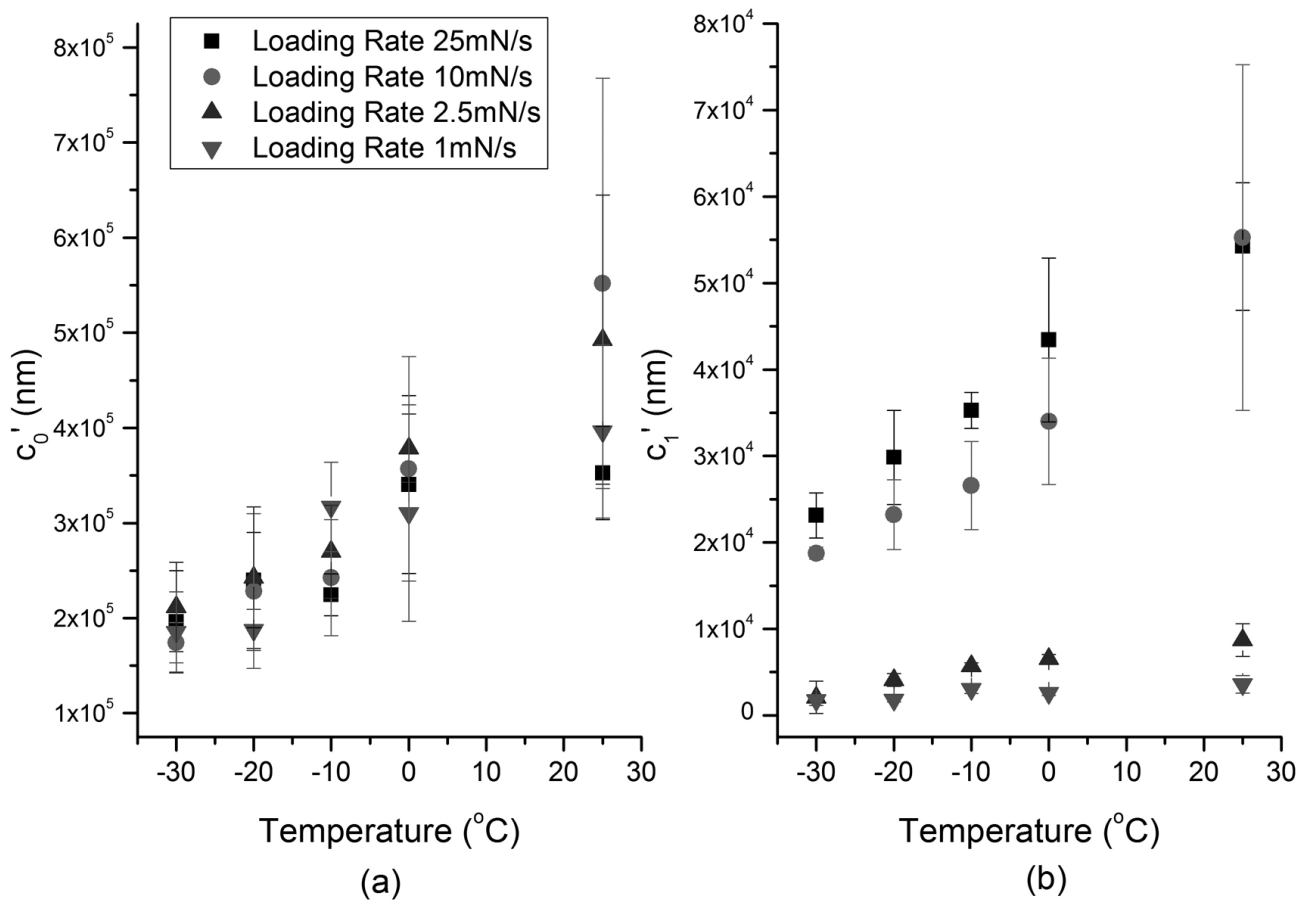


Figure 10 (Figure10(a)_ (b).tif)

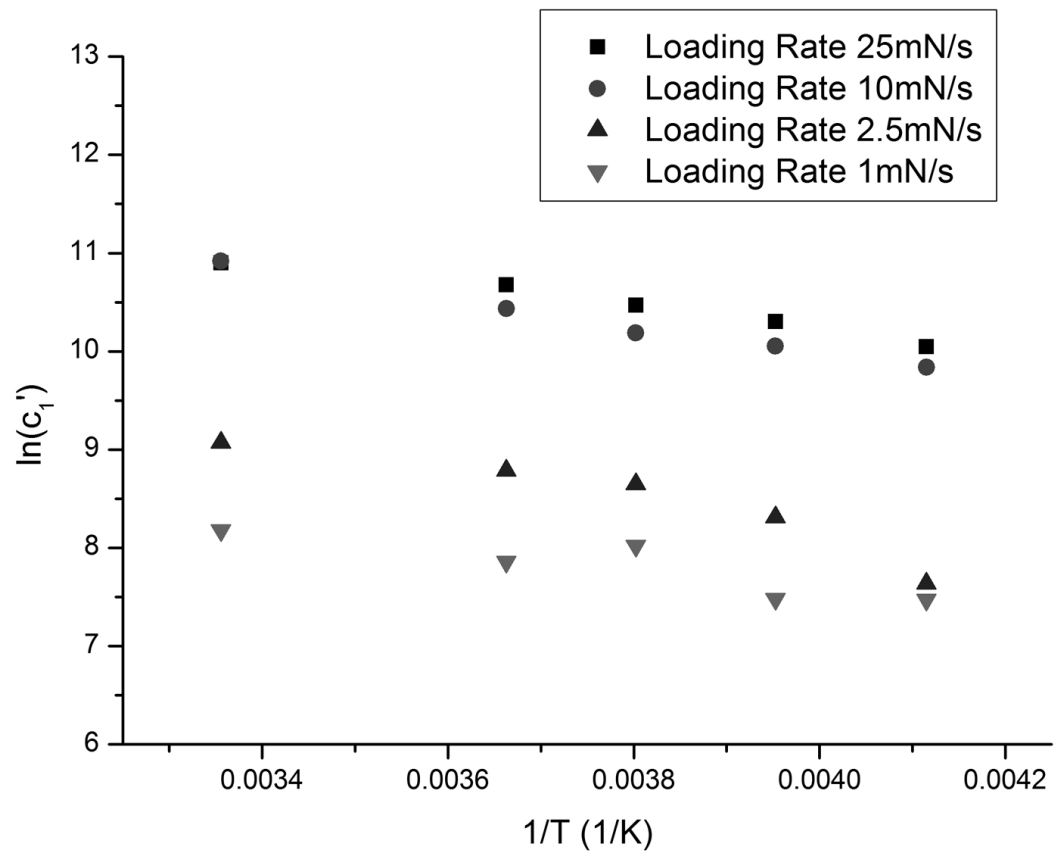


Figure 11 (Figure11.tif)